

See discussions, stats, and author profiles for this publication at: <https://www.researchgate.net/publication/280584329>

Efficient Light Harvester Layer Prepared by Solid/Mist Interface Reaction for Perovskite Solar Cells

ARTICLE in ACS APPLIED MATERIALS & INTERFACES · JULY 2015

Impact Factor: 6.72 · DOI: 10.1021/acsaami.5b04563 · Source: PubMed

READS

36

7 AUTHORS, INCLUDING:



Xiang Xia

Jilin University

4 PUBLICATIONS 0 CITATIONS

[SEE PROFILE](#)



Wu Wenyi

Jilin University

3 PUBLICATIONS 0 CITATIONS

[SEE PROFILE](#)



Chunxiao Gao

Jilin University

146 PUBLICATIONS 975 CITATIONS

[SEE PROFILE](#)



Xizhe Liu

Jilin University

26 PUBLICATIONS 890 CITATIONS

[SEE PROFILE](#)

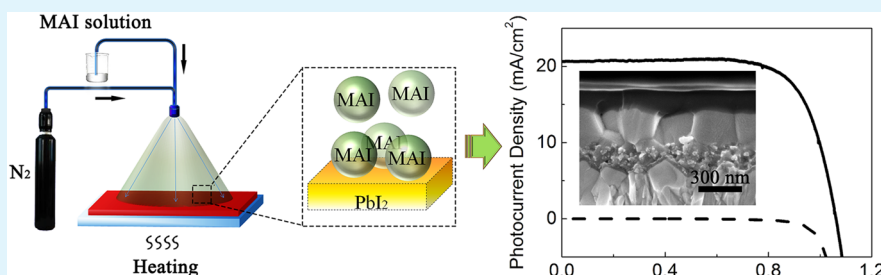
Efficient Light Harvester Layer Prepared by Solid/Mist Interface Reaction for Perovskite Solar Cells

Xiang Xia,[†] Hongcui Li,[†] Wenyi Wu,[‡] Yanhua Li,[†] Dehou Fei,[†] Chunxiao Gao,^{*,‡} and Xizhe Liu^{*,†}

[†]Institute of Atomic and Molecular Physics, Jilin Provincial Key Laboratory of Applied Atomic and Molecular Spectroscopy, and

[‡]State Key Laboratory for Superhard Materials, Jilin University, Changchun, 130012, China

Supporting Information



ABSTRACT: A solid/mist reaction method is developed to produce well-crystallized light harvester layers without pinhole defects for perovskite solar cells. The reaction based on mist precursor can be facilely operated with low process temperature. And it can effectively control the volume of CH₃NH₃I solution and the reaction temperature, which affect the quality of perovskite harvester layers and the performance of perovskite solar cells remarkably. Under optimized condition, the efficiencies of devices reach 16.2% with the average efficiency of 14.9%. The solid/mist reaction is also used to fabricate planar junction solar cells and a PCE of 14.9% is obtained.

KEYWORDS: solar cells, perovskite formation process, morphology-control, low-temperature fabrication, interface reaction, mist

Hybrid organic/inorganic lead halide, which has a perovskite structure, is a kind of new emerging light harvester materials with excellent photovoltaic performance. This kind of perovskite material is originally developed as soluble semiconductors with high carrier mobility. As it has tunable optical properties, this material is also the effective harvester in perovskite solar cells.^{1,2} By using a solid state heterostructure, perovskite solar cells achieve the light to electrical power conversion efficiencies (PCEs) of 9.7% and 10.9% in 2012.^{3,4} Further improvement on interface and composition leads to the conversion efficiency of 18–20%,^{5,6} which approaches the performance of c-Si solar cells and CIGS solar cells.

CH₃NH₃PbI₃ is a wildly investigated perovskite material for the light harvester layers in perovskite solar cells.^{7–10} It is found that pinhole-free perovskite films with high crystallization benefit the device performance and its reproducibility.^{11–16} Therefore, the fabrication of high-quality perovskite films becomes one of the central topics in perovskite solar cells. CH₃NH₃PbI₃ film is usually synthesized by the reaction between lead iodide (PbI₂) and methylammonium iodide (MAI). Although annealing the composite film of these reactants is a direct method for fabricating CH₃NH₃PbI₃ films, its uncontrollable morphology degrades the reproducibility of the photovoltaic devices.³ As improving the morphology of composite films need additional precise control, fabrication methods based on interface reaction are wildly used.^{14–22}

Perovskite films can be fabricated by the solid/liquid^{17,18} interface reaction between PbI₂ film and MAI solution. This solution-based method is wildly used for its facile operation and low process temperature. However, pinhole defects exist on the perovskite films, which leads to the relatively low average PCE (12.0%) of solar cells.¹⁷ As PbI₂ film is dipped in the MAI solution in this reaction, the direct contact between PbI₂ film and MAI solution limits the precise control of solution volume. The modified method based on two-step spin-coating procedure can produce well crystallized MAPbI₃ cuboids, but pinhole defects still exist.¹⁸ The direct contact between PbI₂ film and MAI solution also limits the optimization of reaction temperature, because the temperature affects the solubility of perovskite material in the MAI solution.

Perovskite film can also be fabricated by the reaction at solid/vapor interface. By transporting MAI vapor in inert carrier gas to the reaction interface, efficient perovskite light harvester film can be prepared, and the p-i-n solar cell and p-free solar cell achieve PCEs of 12.1 and 10.6%, respectively.^{14–16} Chemical vapor deposition technique is also used for fabricating perovskite film at the solid/vapor interface.^{19,20} In this method, PbI₂ film was separated from MAI source. In this way, the separately control on the reaction temperature can be

Received: May 26, 2015

Accepted: July 30, 2015

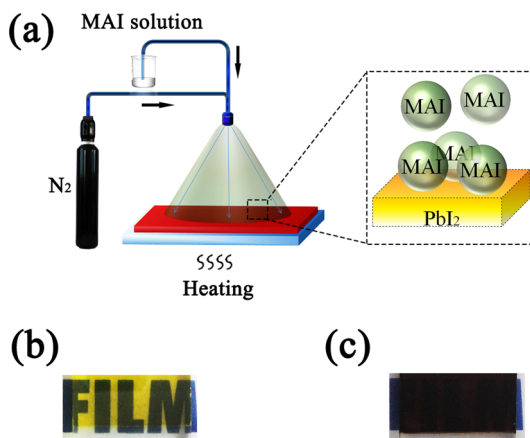
performed. Comparing with solution-based method, the vapor-based method usually needs a relatively high process temperature, but the reaction is still slow. It implies that solvent plays an essential role on the formation and crystallization of perovskite film at low temperature.

Spray technique can generate mist, which is a different precursor from solution and vapor. As spray is a widely used technique, interface reaction based on mist precursor can be facilely operated in industry productions. $\text{MAPbI}_{3-x}\text{Cl}_x$ and MAPbI_3 films are prepared by spraying the mixed solution of MAI and lead halides, and corresponding devices achieve the efficiencies of 11.1 and 10.2%, respectively.^{23,24} These one-step deposition methods have the problem of redissolving predeposited films by the solution mist.

In this study, two-step method based on solid/mist interface reaction can solve this problem by adopting a separate solvent for MAI, which does not dissolve PbI_2 or MAPbI_3 . As a modified solution-based method, the solid/mist interface reaction is facilely operated with low process temperature. Instead of direct contact with MAI solution, the MAI microdroplets are transported to the reaction interface by inert carrier gas, which is just like the vapor-based method. In this way, the volume of MAI solution and the reaction temperature can be controlled effectively.

Scheme 1 illustrates the formation process of perovskite film at solid/mist interface. First, the PbI_2 film was heated to the

Scheme 1. (a) Schematic Illustration of Perovskite Film Formation via Solid/Mist Interface Reaction, Photographs of PbI_2 Films (b) before and (c) after the Solid/Mist Reaction



desired temperature on a hot plate. Then, 10 mg/mL MAI in isopropanol solution was nebulized and sprayed on the top of the PbI_2 film by a nitrogen gas atomizing spray nozzle. In this process, the quantity of reactant and the reaction temperature can be facilely controlled by adjusting the sprayed volume of MAI solution and the temperature of hot plate. The photographs of PbI_2 films before and after the solid/mist reaction are shown in **Scheme 1b, c**, respectively. Details for material preparation and device fabrication can be found in the Supporting Information.

In the solid/mist interface reaction, six MAPbI_3 samples are prepared by MAI solutions with different volumes (50, 100, 200, 400, 600, and 1000 μL , respectively), and the reaction temperature is kept at 80 °C. X-ray diffraction (XRD) patterns of these MAPbI_3 films are shown in **Figure 1a**. Meanwhile,

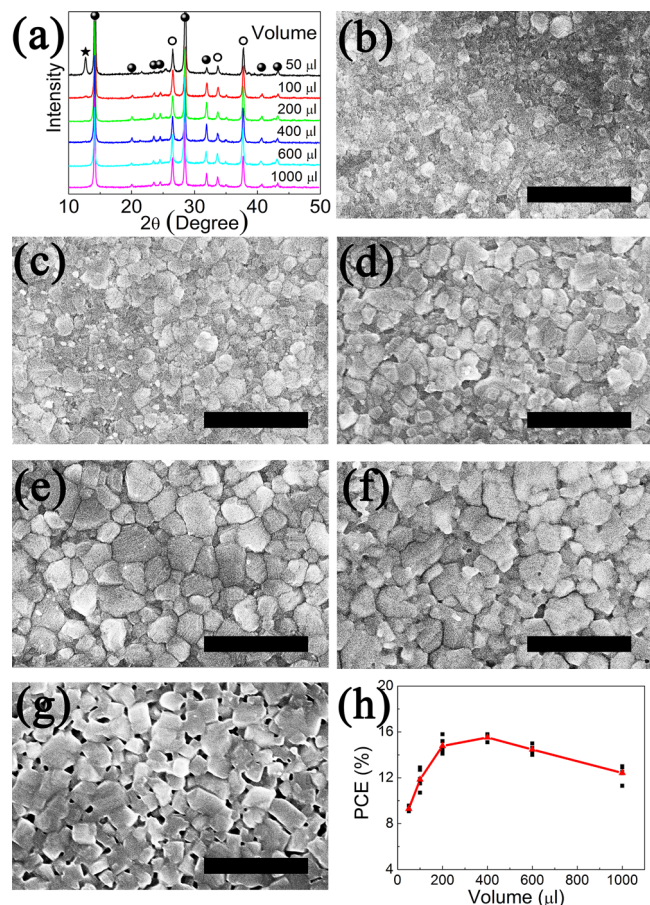


Figure 1. (a) X-ray diffraction (XRD) patterns, (b–g) top-view SEM images, and (h) device efficiency (PCE) of the MAPbI_3 films prepared with various volumes of MAI solution. The XRD peaks assigned to MAPbI_3 , PbI_2 , and FTO crystals are marked with solid circles, asterisks and open circles, respectively. For SEM images, MAI solution volumes are (b) 50, (c) 100, (d) 200, (e) 400, (f) 600, and (g) 1000 μL , and the scale bar is 1 μm .

TiO_2 /FTO substrate, PbI_2 film, and MAI film are measured as the references (**Figure S1**). In the XRD patterns of the MAPbI_3 films (**Figure 1a**), a set of strong peaks (marked with solid circle) assigned to MAPbI_3 crystal indicate a tetragonal crystal structure of halide perovskite. Furthermore, an extra strong peak at 12.65° exists in the XRD pattern of the MAPbI_3 film prepared by 50 μL of MAI solution, which belongs to the residual PbI_2 . This indicates that 50 μL of MAI solution is not enough to complete the conversion from PbI_2 to MAPbI_3 . Moreover, the intensity of the PbI_2 characteristic peak attenuates in the MAPbI_3 films prepared by 100 μL of MAI solution, and disappears at 200 μL . All of the MAPbI_3 films prepared by 200–1000 μL of MAI solution show the similar characteristic peaks in the XRD patterns. Therefore, 200 μL of MAI solution is enough for the conversion from PbI_2 to MAPbI_3 . This volume is much lower than that used in solid/liquid reaction.

Scanning electron microscope (SEM) images of the MAPbI_3 films prepared with different volumes of MAI solution are shown in **Figure 1b–g**. As shown in **Figure 1b**, poorly crystallized MAPbI_3 film with nonuniform crystal grain size is prepared by 50 μL of MAI solution. With increasing of MAI solution from 50 to 400 μL , the crystal grains of the MAPbI_3 film are grown (**Figure 1b–e**). Although 200 μL of MAI

solution is enough for converting PbI_2 to MAPbI_3 , a further increase in MAI solution to 400 μL can improve the crystallization of MAPbI_3 film. Previous reports show that DMF vapor and water vapor can enhance the crystal growth of perovskite light harvester films.^{25–27} Although the treatment time is much shorter than that of solvent vapor treatment, the crystal growth in Figure 1b–e implies that solution mist treatment is also an effective technique for improving the crystallization of perovskite films. Comparing with the compact morphology in Figure 1b–e, small pinholes emerge in the MAPbI_3 films prepared by 600 μL of MAI solution (Figure 1f). In Figure 1g, the MAPbI_3 crystal grains distribute loosely, and holes with the size of 50 nm appear in the film prepared by 1000 μL of MAI solution. It is found that the excessive MAI solution leads to a polyhedral shape of the MAPbI_3 crystal grains (Figure 1g), which is just like the crystal grains prepared by the solid/liquid reaction (Figure S2). Therefore, the volume of MAI solution is an important factor for controlling the morphology of MAPbI_3 films.

The PCEs of the devices based on these MAPbI_3 films are summarized in Figure 1h, and the photovoltaic parameters are summarized in Table S1. For each solution volume, five devices are fabricated. As shown in Figure 1h, the devices fabricated with 50 μL of MAI solution give the lowest average efficiency of 9.3%. The average efficiency increases to 11.9 and 14.8% when MAI solution is increased to 100 and 200 μL , respectively. For the MAPbI_3 film prepared with 400 μL of MAI solution, the corresponding devices achieve the highest average efficiency of 15.5%, and its uncertainty is the lowest one among six fabrication conditions. SEM images and XRD patterns show that MAPbI_3 crystal grains are grown and residual PbI_2 are decreased by the increment of MAI solution from 50 to 400 μL . As a consequence, the grain boundaries and defects of the MAPbI_3 film are reduced, and the lifetime and mobility of charge carriers can be improved.^{11,12} As the volume of MAI solution further increases to 600 μL and 1000 μL , the average efficiency reduces to 14.5% and 12.4% respectively. SEM images (Figure 1f and g) show that pinholes emerge in the MAPbI_3 film prepared under these conditions. These pinholes can provide the shunt path for leakage current, which leads to the decrease on fill factor and short circuit current density (J_{SC}) (Table S1).^{15,28}

The solid/mist interface reaction permits the control of reaction temperature without disturbing the temperature of MAI solution source. Six reaction temperatures (40, 60, 80, 100, 120, and 140 °C, respectively) are applied to study the effect of reaction temperature in the formation of MAPbI_3 film. The volume of MAI solution is kept at 400 μL . The XRD patterns of the MAPbI_3 films prepared at various reaction temperatures are shown in Figure 2a. At the reaction temperature of 40 °C, XRD pattern of the prepared film gives a diffraction peak at 12.65°, which belongs to unreacted PbI_2 . Low reaction temperature leads to low reaction rate between PbI_2 and MAI, which results in the residual PbI_2 existed after the reaction. When reaction temperature increases to the range from 60 to 120 °C, the absence of PbI_2 characteristic peak suggests the complete conversion from PbI_2 to MAPbI_3 . Furthermore, at high reaction temperatures of 140 °C, PbI_2 characteristic peak reappears, which comes from the thermal decomposition of MAPbI_3 .

SEM images of the MAPbI_3 films prepared at different reaction temperatures are shown in Figure 2b–g. Figure 2b shows the MAPbI_3 film prepared at 40 °C, which exhibits poor

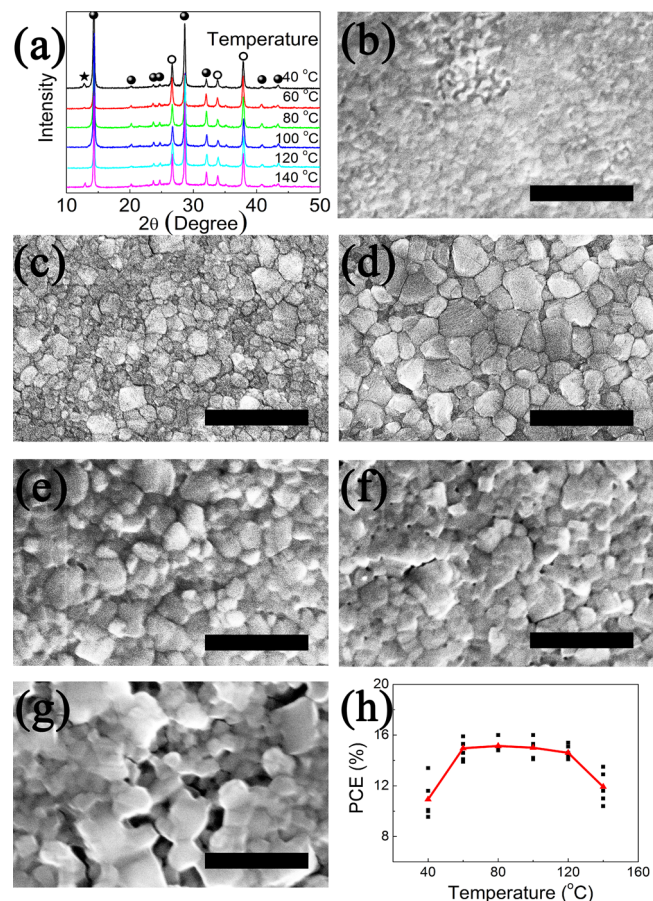


Figure 2. (a) X-ray diffraction (XRD) patterns, (b–g) top-view SEM images, and (h) device efficiency (PCE) of the MAPbI_3 films prepared at various reaction temperatures. The XRD peaks assigned to MAPbI_3 , PbI_2 , and FTO crystals are marked with solid circles, asterisks, and open circles, respectively. For SEM images, the reaction temperatures are (b) 40, (c) 60, (d) 80, (e) 100, (f) 120, and (g) 140 °C, the scale bar is 1 μm .

crystallinity. After increasing the reaction temperature to the range from 60 to 100 °C, the prepared MAPbI_3 films have compact structure, but perovskite crystal grains are different in size (Figure 2c–e). Large perovskite crystal grains are obtained at high reaction temperature. This result means that the growth rate of perovskite crystal is faster at higher temperature. Some unobvious pinholes appear in the MAPbI_3 film prepared at 120 °C (Figure 2f), and further increase of the reaction temperature (140 °C) makes pinholes into obvious holes (Figure 2g). Therefore, reaction temperature not only determines the composition but also the morphology of MAPbI_3 films.

The PCEs of the devices based on the MAPbI_3 films prepared at different temperature are summarized in Figure 2h, and the photovoltaic parameters are summarized in Table S2. For the reaction temperature of 40 °C, the devices have a relatively low average efficiency of 10.9%. XRD and SEM analysis (Figure 2a, b) indicate that poorly crystallized MAPbI_3 film with residual PbI_2 is produced at 40 °C. These structure defects can block the transport of charge carriers and facilitate the recombination process in the device.^{11,12} As shown in the above discussion, increasing reaction temperature can improve the crystallization of MAPbI_3 films and eliminate residual PbI_2 . Highly efficient devices (~15% in PCE) can be fabricated at the reaction temperature between 60 and 120 °C. In the reports of

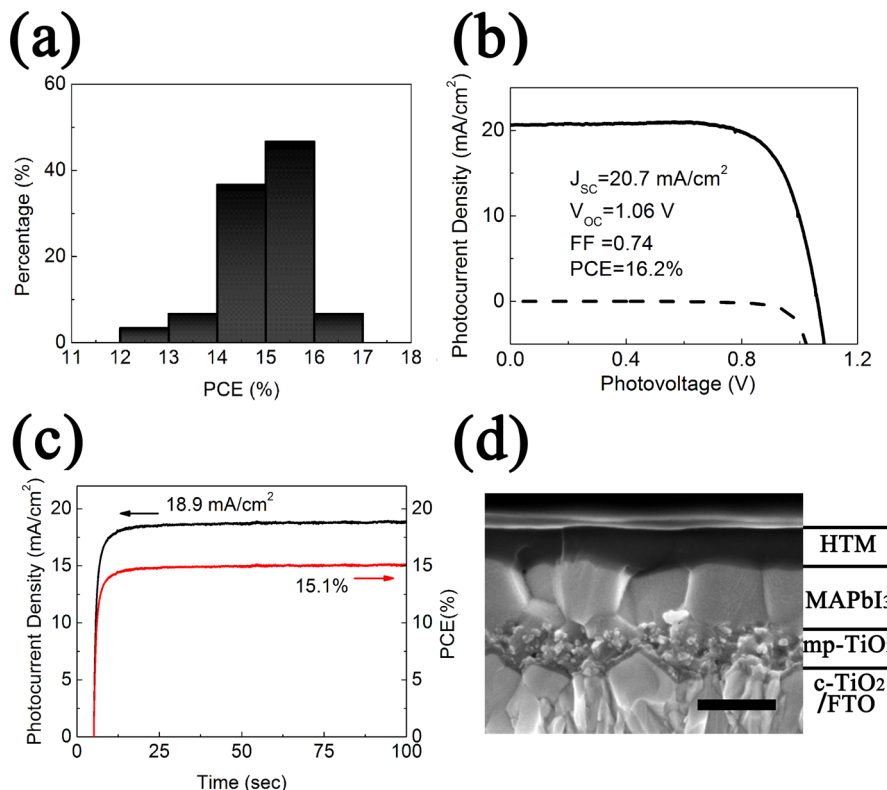


Figure 3. (a) Device performance statistics based on 30 devices, (b) photocurrent density–photovoltage characteristic of the best-performing device (solid line) and the dark I – V curve (dash line), (c) steady-state current measured at a forward bias of 0.80 V and stabilized power output, (d) cross-sectional SEM image of the device, mp-TiO₂ represents the mesoporous TiO₂ layer penetrated with MAPbI₃, c-TiO₂ represents the compact TiO₂ layer, the scale bar is 300 nm.

solid/vapor methods, the reactions are usually conducted at 120–150 °C for 1–2 h.^{14–16} On the contrary, solid/mist reaction can be performed at 60 °C, and the reaction can complete in 2 min. Therefore, solid/mist method is a facile low temperature method with high throughput. After further increasing the reaction temperature to 140 °C, PCEs of the devices remarkable decrease to 11.9%. At high reaction temperature, the MAPbI₃ film is partially decomposed (Figure 2a) and pinhole defects (Figure 2g) exist in the film. The damaged light harvester film leads to an obvious decrease in J_{SC} . And the porous nature of the high temperature prepared MAPbI₃ film increases the leakage current between TiO₂ and hole conductor.^{15,28}

The solid/mist reaction method can produce high-quality MAPbI₃ films by the facile control of reaction conditions. We fabricate a series of 30 devices under the optimized condition of 400 μL MAI solution and 80 °C. The statistics of PCEs based on the 30 devices is shown in Figure 3a. More than 90% of the devices achieve an efficiency of above 14%. It indicates that this solid/mist interface reaction method has excellent reproducibility and high performance. The photocurrent density–photovoltage characteristic of the best-performing device is depicted in Figure 3b. The device exhibits outstanding power conversion efficiency of 16.2%, with 20.7 mA/cm² in J_{SC} , 1.06 V in open circuit voltage V_{OC} and 0.74 in fill factor (FF). We also records the photocurrent of a device held at a forward bias of 0.80 V as the function of time to gain some understanding of the stabilized power output under working conditions (Figure 3c). The photocurrent stabilizes within seconds to approximately 18.9 mA/cm², yielding a stabilized power conversion efficiency of 15.1%, measured after 100 s. This indicates that

the devices have good working-stability. Furthermore, this stabilized efficiency is closer to the efficiency measured via reverse scan (15.8%) than that via forward scan (13.6%) (Figure S3). It implies that reverse scan can provide a relatively accurate representation of the photovoltaic performance for this kind of devices. The cross-sectional SEM image of a device is shown in Figure 3d. Highly crystallized MAPbI₃ capping layer without pinhole defects covers on mesoporous TiO₂ layer. The MAPbI₃ grains in the capping layer are so large that a single grain can connect the TiO₂ layer and the hole conductor layer. The elimination of grain boundaries can alleviate carrier recombination and facilitate charge transport in the MAPbI₃ layer.^{11,12}

Furthermore, planar junction perovskite solar cells are also fabricated using this solid/mist interface reaction (Figure S4). Planar junction device is attractive for its simple device structure, but pinhole free perovskite film with high crystallization is necessary to prevent the leakage current and enhance the carrier diffusion.^{28–32} The excellent efficiency of 14.9% confirms the availability of the solid/mist method.

In summary, we develop a solid/mist interface reaction method to fabricate CH₃NH₃PbI₃ light harvester film for perovskite solar cells. In this method, high-quality CH₃NH₃PbI₃ films can be prepared at low temperature, and reaction conditions can be facilely controlled. Detail studies reveal that the volume of CH₃NH₃I solution and the reaction temperature control not only the extent of reaction but also the morphology and crystallization of the CH₃NH₃PbI₃ film. Under optimized conditions, pinhole-free CH₃NH₃PbI₃ films with high crystallization can be obtained, and the PCEs of corresponding devices reach 16.2% with the average efficiency

of 14.9%. This method is also effective for fabricating planar junction perovskite solar cells. This reaction based on mist precursor is enlargeable with high throughput, which is suitable for industrial application. We think that this solid/mist reaction can be a general method for fabricating perovskite light harvester films, and it also has potential in other compound films.

ASSOCIATED CONTENT

Supporting Information

The Supporting Information is available free of charge on the ACS Publications website at DOI: [10.1021/acsami.5b04563](https://doi.org/10.1021/acsami.5b04563).

Experimental details, device photovoltaic parameters, XRD patterns for references, SEM images for references, *I*–*V* characteristic via different scanning directions, *I*–*V* characteristic of the planar junction device, the effect of MAI solution concentration, comparison of Ag and Au top electrode, IPCE spectrum ([PDF](#))

AUTHOR INFORMATION

Corresponding Author

*E-mail: liu_xizhe@jlu.edu.cn.

Notes

The authors declare no competing financial interest.

ACKNOWLEDGMENTS

This work was partially supported by National Science Foundation of China (Grants 51273079, 11374121), National Basic Research Program of China (Grant 2011CB808204), the Science Development Program of Jilin Province (Grant 20150519021JH), and the Fundamental Research Funds for Central Universities at Jilin University.

REFERENCES

- (1) Kojima, A.; Teshima, K.; Shirai, Y.; Miyasaka, T. Organometal Halide Perovskites as Visible-Light Sensitizers for Photovoltaic Cells. *J. Am. Chem. Soc.* **2009**, *131*, 6050–6051.
- (2) Im, J.; Lee, C.; Lee, J.; Park, S.; Park, N. 6.5% Efficient Perovskite Quantum-Dot-Sensitized Solar Cell. *Nanoscale* **2011**, *3*, 4088–4093.
- (3) Kim, H.; Lee, C.; Im, J.; Lee, K.; Moehl, T.; Marchioro, A.; Moon, S.; Humphry-Baker, R.; Yum, J.; Moser, J.; Grätzel, M.; Park, N. Lead Iodide Perovskite Sensitized All-Solid-State Submicron Thin Film Mesoscopic Solar Cell with Efficiency Exceeding 9%. *Sci. Rep.* **2012**, *2*, 591.
- (4) Lee, M.; Teuscher, J.; Miyasaka, T.; Murakami, T.; Snaith, H. Efficient Hybrid Solar Cells Based on Meso-Superstructured Organometal Halide Perovskites. *Science* **2012**, *338*, 643–647.
- (5) Zhou, H.; Chen, Q.; Li, G.; Luo, S.; Song, T.; Duan, H. S.; Hong, Z.; You, J.; Liu, Y.; Yang, Y. Interface Engineering of Highly Efficient Perovskite Solar Cells. *Science* **2014**, *345*, 542–546.
- (6) Jeon, N.; Noh, J.; Yang, W.; Kim, Y.; Ryu, S.; Seo, J.; Seok, S. Compositional Engineering of Perovskite Materials for High-Performance Solar Cells. *Nature* **2015**, *517*, 476–480.
- (7) Yin, X.; Guo, Y.; Xue, Z.; Xu, P.; He, M.; Liu, B. Performance Enhancement of Perovskite-Sensitized Mesoscopic Solar Cells Using Nb-Doped TiO₂ Compact Layer. *Nano Res.* **2015**, *8*, 1997–2003.
- (8) Etgar, L.; Gao, P.; Xue, Z.; Peng, Q.; Chandiran, A.; Liu, B.; Nazeeruddin, M. K.; Grätzel, M. Mesoscopic CH₃NH₃PbI₃/TiO₂ Heterojunction Solar Cells. *J. Am. Chem. Soc.* **2012**, *134*, 17396–17399.
- (9) Hu, Q.; Wu, J.; Jiang, C.; Liu, T.; Que, X.; Zhu, R.; Gong, Q. Engineering of Electron-Selective Contact for Perovskite Solar Cells with Efficiency Exceeding 15%. *ACS Nano* **2014**, *8*, 10161–10167.
- (10) Xiao, J.; Shi, J.; Liu, H.; Xu, Y.; Lv, S.; Luo, Y.; Li, D.; Meng, Q.; Li, Y. Efficient CH₃NH₃PbI₃ Perovskite Solar Cells Based on Graphdiyne(GD)-Modified P3HT Hole-Transporting Material. *Adv. Energy Mater.* **2015**, *5*, 1401943.
- (11) Nie, W.; Tsai, H.; Asadpour, R.; Blancon, J.; Neukirch, A.; Gupta, G.; Crochet, J.; Chhowalla, M.; Tretiak, S.; Alam, M.; Wang, H.; Mohite, A. High-Efficiency Solution-Processed Perovskite Solar Cells with Millimeter-Scale Grains. *Science* **2015**, *347*, 522–525.
- (12) deQuilettes, D.; Vorpahl, S.; Stranks, S.; Nagaoka, H.; Eperon, G.; Ziffer, M. E.; Snaith, H.; Ginger, D. Solar cells. Impact of Microstructure on Local Carrier Lifetime in Perovskite Solar Cells. *Science* **2015**, *348*, 683–686.
- (13) Heo, J.; Song, D.; Han, H.; Kim, S.; Kim, J.; Kim, D.; Shin, H.; Ahn, T.; Wolf, C.; Lee, T.; Im, S. Planar CH₃NH₃PbI₃ Perovskite Solar Cells with Constant 17.2% Average Power Conversion Efficiency Irrespective of the Scan Rate. *Adv. Mater.* **2015**, *27*, 3424–3430.
- (14) Chen, Q.; Zhou, H.; Hong, Z.; Luo, S.; Duan, H. S.; Wang, H. H.; Liu, Y. S.; Li, G.; Yang, Y. Planar Heterojunction Perovskite Solar Cells via Vapor-Assisted Solution Process. *J. Am. Chem. Soc.* **2014**, *136*, 622–625.
- (15) Hao, F.; Stoumpos, C. C.; Liu, Z.; Chang, R.; Kanatzidis, M. Controllable Perovskite Crystallization at a Gas-Solid Interface for Hole Conductor-Free Solar Cells with Steady Power Conversion Efficiency over 10%. *J. Am. Chem. Soc.* **2014**, *136*, 16411–16419.
- (16) Li, Y.; Cooper, J.; Buonsanti, R.; Giannini, C.; Liu, Y.; Toma, F.; Sharp, I. Fabrication of Planar Heterojunction Perovskite Solar Cells by Controlled Low-Pressure Vapor Annealing. *J. Phys. Chem. Lett.* **2015**, *6*, 493–499.
- (17) Burschka, J.; Pellet, N.; Moon, S.; Humphry-Baker, R.; Gao, P.; Nazeeruddin, M.; Grätzel, M. Sequential Deposition as a Route to High-Performance Perovskite-Sensitized Solar Cells. *Nature* **2013**, *499*, 316–319.
- (18) Im, J.; Jang, I.; Pellet, N.; Grätzel, M.; Park, N. Growth of CH₃NH₃PbI₃ Cuboids with Controlled Size for High-Efficiency Perovskite Solar Cells. *Nat. Nanotechnol.* **2014**, *9*, 927–932.
- (19) Leyden, M.; Ono, L.; Raga, S.; Kato, Y.; Wang, S.; Qi, Y. High Performance Perovskite Solar Cells by Hybrid Chemical Vapor Deposition. *J. Mater. Chem. A* **2014**, *2*, 18742–18745.
- (20) Luo, P.; Liu, Z.; Xia, W.; Yuan, C.; Cheng, J.; Lu, Y. Uniform, Stable, and Efficient Planar-Heterojunction Perovskite Solar Cells by Facile Low-Pressure Chemical Vapor Deposition under Fully Open-Air Conditions. *ACS Appl. Mater. Interfaces* **2015**, *7*, 2708–2714.
- (21) Xu, Y.; Zhu, L.; Shi, J.; Lv, S.; Xu, X.; Xiao, J.; Dong, J.; Wu, H.; Luo, Y.; Li, D.; Meng, Q. Efficient Hybrid Mesoscopic Solar Cells with Morphology-Controlled CH₃NH₃PbI_{3-x}Cl_x Derived from Two-Step Spin Coating Method. *ACS Appl. Mater. Interfaces* **2015**, *7*, 2242–2248.
- (22) Shi, J.; Luo, Y.; Wei, H.; Luo, J.; Dong, J.; Lv, S.; Xiao, J.; Xu, Y.; Zhu, L.; Xu, X.; Wu, H.; Li, D.; Meng, Q. Modified Two-Step Deposition Method for High-Efficiency TiO₂/CH₃NH₃PbI₃ Heterojunction Solar Cells. *ACS Appl. Mater. Interfaces* **2014**, *6*, 9711–9718.
- (23) Barrows, A.; Pearson, A.; Kwak, C.; Dunbar, A.; Buckley, A.; Lidzey, D. Efficient Planar Heterojunction Mixed-halide Perovskite Solar Cells Deposited via Spray Deposition. *Energy Environ. Sci.* **2014**, *7*, 2944–2950.
- (24) Ramesh, M.; Boopathi, K.; Huang, T.; Huang, Y.; Tsao, C.; Chu, C. Using an Airbrush Pen for Layer-by-Layer Growth of Continuous Perovskite Thin Films for Hybrid Solar Cells. *ACS Appl. Mater. Interfaces* **2015**, *7*, 2359–2366.
- (25) Xiao, Z.; Dong, Q.; Bi, C.; Shao, Y.; Yuan, Y.; Huang, J. Solvent Annealing of Perovskite-Induced Crystal Growth for Photovoltaic-Device Efficiency Enhancement. *Adv. Mater.* **2014**, *26*, 6503–6509.
- (26) You, J.; Yang, Y.; Hong, Z.; Song, T. B.; Meng, L.; Liu, Y.; Jiang, C.; Zhou, H.; Chang, W. H.; Li, G.; Yang, Y. Moisture Assisted Perovskite Film Growth for High Performance Solar Cells. *Appl. Phys. Lett.* **2014**, *105*, 183902.
- (27) Zhu, W.; Yu, T.; Li, F.; Bao, C.; Gao, H.; Li, Y.; Yang, J.; Fu, G.; Zhou, X.; Zou, Z. A Facile, Solvent Vapor-Fumigation-Induced, Self-

Repair Recrystallization of $\text{CH}_3\text{NH}_3\text{PbI}_3$ Films for High-Performance Perovskite Solar Cells. *Nanoscale* **2015**, *7*, 5427–5434.

(28) Eperon, G.; Burlakov, V.; Docampo, P.; Goriely, A.; Snaith, H. Morphological Control for High Performance, Solution-Processed Planar Heterojunction Perovskite Solar Cells. *Adv. Funct. Mater.* **2014**, *24*, 151–157.

(29) Jeon, N.; Noh, J.; Kim, Y.; Yang, W.; Ryu, S.; Seok, S. Solvent Engineering for High-Performance Inorganic-Organic Hybrid Perovskite Solar Cells. *Nat. Mater.* **2014**, *13*, 897–903.

(30) Wu, Y.; Islam, A.; Yang, X.; Qin, C.; Liu, J.; Zhang, K.; Peng, W.; Han, L. Retarding the Crystallization of PbI_2 for Highly Reproducible Planar-Structured Perovskite Solar Cells via Sequential Deposition. *Energy Environ. Sci.* **2014**, *7*, 2934–2938.

(31) Xiao, M.; Huang, F.; Huang, W.; Dkhissi, Y.; Zhu, Y.; Etheridge, J.; Weale, A.; Bach, U.; Cheng, Y.; Spiccia, L. A Fast Deposition-Crystallization Procedure for Highly Efficient Lead Iodide Perovskite Thin-Film Solar Cells. *Angew. Chem., Int. Ed.* **2014**, *53*, 9898–9903.

(32) Zhang, W.; Saliba, M.; Moore, D.; Pathak, S.; Horantner, M.; Stergiopoulos, T.; Stranks, S.; Eperon, G.; Alexander-Webber, J.; Abate, A.; Sadhanala, A.; Yao, S.; Chen, Y.; Friend, R.; Estroff, L.; Wiesner, U.; Snaith, H. Ultrasmooth Organic-Inorganic Perovskite Thin-Film Formation and Crystallization for Efficient Planar Heterojunction Solar Cells. *Nat. Commun.* **2015**, *6*, 6142.

Supporting Information

Efficient Light Harvester Layer Prepared by Solid/Mist Interface Reaction for Perovskite Solar Cells

Xiang Xia,^a Hongcui Li,^a Wenyi Wu,^b Yanhua Li,^a Dehou Fei,^a Chunxiao Gao^{b,*}

and Xizhe Liu^{a,*}

^aJilin Provincial Key Laboratory of Applied Atomic and Molecular Spectroscopy, Institute of Atomic and Molecular Physics, Jilin University, Changchun, 130012, China

^bState Key Laboratory for Superhard Materials, Jilin University, Changchun, 130012, China

AUTHOR INFORMATION

Corresponding Author

*E-mail: (L. X.) liu_xizhe@jlu.edu.cn

*E-mail: (G. C.) gaocx@jlu.edu.cn

1. Experimental Section

Preparation of methylammonium iodine (MAI): MAI was synthesized by reacting 17.90 ml CH₃NH₂ (33 wt% in ethanol) and 22.84 ml HI (47 wt% in water) in a round-bottom flask at 0 °C for 4 h with stirring. Then, crude MAI power was obtained from the mixed solution by evaporation. Finally, the crude MAI power was dissolved in ethanol, recrystallized from diethyl ether, and dried at 60 °C in a vacuum oven for 12 h to get white MAI power.

Fabrication of perovskite solar cells: Firstly, fluorine doped tin oxide (FTO) glass was etched and cleaned. Then, compact TiO₂ film (c-TiO₂, ~30 nm in thickness) was deposited by spray pyrolysis with 50 mmol/L Ti(OPr)₂(AcAc)₂ in ethanol solution at 450 °C. Mesoporous TiO₂ film (mp-TiO₂) was deposited on the c-TiO₂ film by spin-coating with ethanol diluted TiO₂ paste (18NRT, Dyesol) solution at 5000 rpm for 30 sec. The mass ratio of TiO₂ paste to ethanol is 1:6. Then, the sample was dried and sintered at 80 °C for 30 min, 125 °C for 30 min, 325 °C for 30 min, and 500 °C for 30 min. After further treatment with 40 mM TiCl₄ at 70 °C for 30 min, the sample was rinsed with water and ethanol, and sintered at 450 °C for 30 min. Then, PbI₂ film was prepared on the sample by spin-coating with 462 mg/ml PbI₂ in N,N-Dimethylformamide solution at 4000 rpm for 30 sec. After drying and preheating at the desired reaction temperature for 5 min on a hot plate, 10 mg/ml MAI in isopropanol solution was nebulized and sprayed on the top of the PbI₂ film by a nitrogen gas atomizing spray nozzle. After spin-coating PbI₂ solution, the PbI₂ film was directly preheated at the same temperature of the following Solid/Mist reaction. No extra drying procedure was applied. To control the quality of mist, the

spraying speed of MAI solution was constant ($5 \mu\text{l/s}$) and the flow rate of N_2 gas was also constant (200 L/h). Therefore, the corresponding spraying time was 10 s , 20 s , 40 s , 80 s , 120 s , and 200 s for $50 \mu\text{l}$, $100 \mu\text{l}$, $200 \mu\text{l}$, $400 \mu\text{l}$, $600 \mu\text{l}$ and $1000 \mu\text{l}$ MAI solution, respectively. All of these MAI solutions were sprayed continuously in one time. The working distance between spray nozzle and PbI_2 film was 8 cm . The area of one PbI_2 film sample and its substrate was $1.2 \text{ cm} * 1.5 \text{ cm}$ and $1.5 \text{ cm} * 1.5 \text{ cm}$, respectively. The spraying area on the hot plate was about 24 cm^2 . Different volumes of MAI solution and different reaction temperatures were applied. After another 10 min heating, the film was washed with isopropanol and annealed at 70°C for 30 min . The hole conductor layer was then deposited by spin-coating at $4,000 \text{ rpm}$ for 20 sec . The spin-coating solution was prepared by dissolving 72.3 mg ($2,2',7,7'$ -tetrakis(N,N -di-p-methoxyphenylamine)- $9,9$ -spirobifluorene) (spiro-MeOTAD), 28.8 ul 4-tert-butylpyridine and 17.5 ul lithium bis(trifluoromethylsulphonyl)imide solution (520 mg/ml in acetonitrile) in 1 ml chlorobenzene. After spiro-MeOTAD being aged in the dried air condition of a brown desiccator for 12 hours , silver electrode was deposited to complete the device. All these operations were performed in air condition.

Characterization: The SEM images were investigated by FEI MAGELLAN 400 Scanning Electron Microscope. The X-ray diffraction (XRD) spectra were obtained using a Rigaku D/max-2550 X-ray diffractometer. Photocurrent density-photovoltage characteristics were recorded from 1.15 V to 0 V by a CHI660 electrochemical workstation. The active area of solar cells was 0.15 cm^2 , which defined by a mask. AM1.5 illumination was provided by a 3A class

solar simulator (UHE-16, ScienceTech Inc.), which was calibrated to one sun by a KG5 filtered Si reference solar cell (certificated by VLSI Standards Inc., traceable to National Renewable Energy Laboratory). IPCE spectra are measured in the DC mode by a controlled monochrometer (BOCIC Inc.) with a 300W Xe light source (NBet Inc.). The certificated Si cell (VLSI Standards Inc.) is used as the reference.

2. Table

Table S1. The photovoltaic parameters of the devices prepared by MAI solutions with different volumes

Volume	Device NO.	J_{sc} (mA/cm ²)	V_{oc} (V)	Fill factor	PCE (%)
50 ul	1	13.8	1.08	0.62	9.30
	2	13.3	1.07	0.65	9.29
	3	12.9	1.06	0.66	9.08
	4	13.4	1.05	0.68	9.58
	5	13.3	1.05	0.66	9.20
100 ul	1	17.9	1.06	0.68	12.9
	2	16.1	1.05	0.68	11.5
	3	15.4	1.06	0.66	10.7
	4	17.0	1.08	0.65	11.9
	5	17.9	1.07	0.66	12.7
200 ul	1	20.1	1.09	0.69	15.2
	2	20.5	1.09	0.71	15.8
	3	19.1	1.08	0.70	14.4
	4	19.2	1.08	0.70	14.5
	5	19.4	1.08	0.67	14.1
400 ul	1	20.2	1.08	0.71	15.5
	2	20.6	1.08	0.70	15.6
	3	20.6	1.09	0.70	15.8
	4	20.9	1.09	0.68	15.6
	5	21.3	1.09	0.65	15.1
600 ul	1	19.2	1.08	0.70	14.5
	2	19.7	1.08	0.67	14.2
	3	19.7	1.07	0.69	14.6
	4	19.5	1.09	0.71	15.0
	5	19.7	1.08	0.66	14.0
1000 ul	1	17.6	1.08	0.68	13.0
	2	17.4	1.07	0.69	12.9
	3	17.5	1.07	0.67	12.5
	4	16.9	1.08	0.68	12.4
	5	16.5	1.03	0.66	11.3

Table S2. The photovoltaic parameters of the devices prepared at different reaction temperatures

Temperature	Device NO.	J_{sc} (mA/cm ²)	V_{oc} (V)	Fill factor	PCE (%)
40 °C	1	21.0	1.03	0.62	13.4
	2	18.1	1.07	0.60	11.6
	3	18.0	1.00	0.56	10.1
	4	16.9	0.95	0.62	10.0
	5	17.5	0.94	0.58	9.55
60 °C	1	21.7	1.11	0.66	15.9
	2	21.4	1.08	0.66	15.3
	3	18.4	1.09	0.69	13.9
	4	19.9	1.06	0.67	14.1
	5	20.3	1.06	0.68	14.6
80 °C	1	19.5	1.08	0.71	14.9
	2	19.8	1.08	0.70	15.0
	3	20.3	1.09	0.68	15.0
	4	20.4	1.07	0.68	14.8
	5	21.9	1.07	0.68	16.0
100 °C	1	21.2	1.08	0.70	16.0
	2	20.1	1.04	0.68	14.2
	3	20.0	1.07	0.71	15.2
	4	21.7	1.08	0.65	15.3
	5	19.6	1.07	0.67	14.1
120 °C	1	20.1	1.05	0.72	15.2
	2	21.5	1.00	0.66	14.1
	3	21.0	1.05	0.70	15.4
	4	20.1	1.06	0.68	14.4
	5	21.1	1.06	0.67	15.1
140 °C	1	19.2	0.91	0.59	10.4
	2	18.5	0.91	0.65	11.0
	3	18.4	0.99	0.64	11.6
	4	19.0	0.98	0.69	12.9
	5	18.8	1.02	0.71	13.5

3. Figure

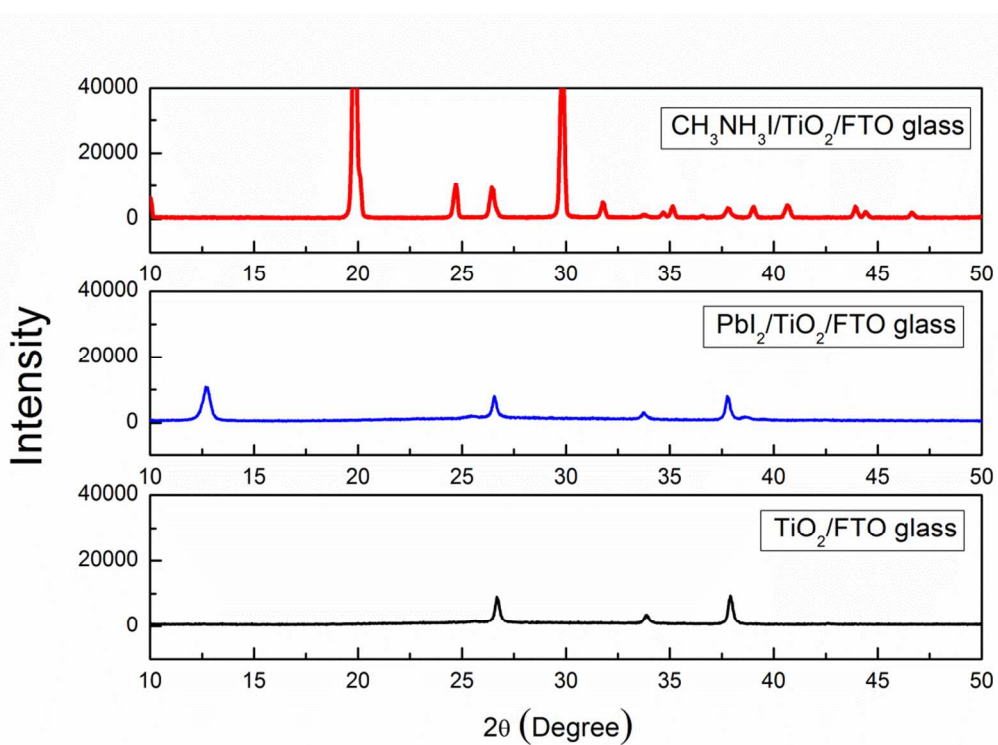


Figure S1. X-ray diffraction (XRD) patterns of MAI/TiO₂/FTO glass, PbI₂/TiO₂/FTO glass and TiO₂/FTO glass.

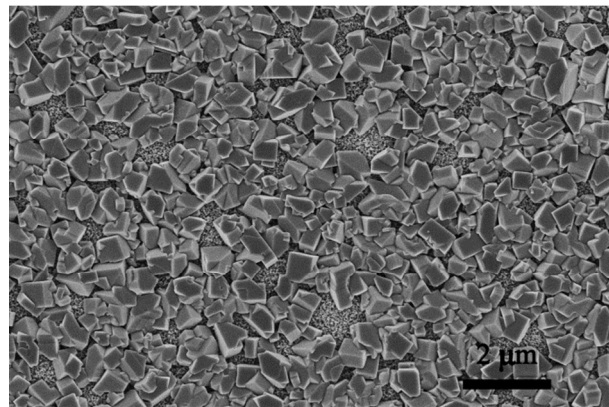


Figure S2. Top-view SEM images of perovskite film obtained by solid/liquid interface reaction.¹ The prepared PbI₂ film was dipped into 10 mg/ml MAI in isopropanol solution for 60 s, and then annealed at 70 °C for 30 min.

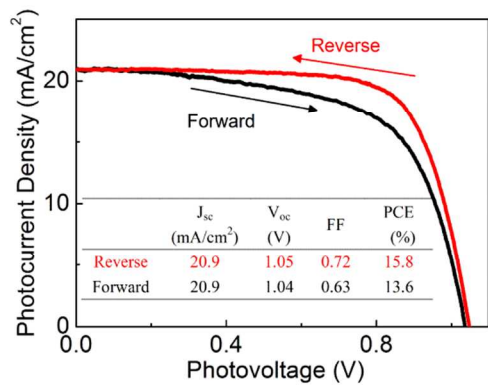


Figure S3. The photocurrent density-photovoltage characteristic of the device via different scanning directions. Reverse scan is the first scan direction (from 1.1 V to 0 V), and the scan rate is 0.1 V/s.

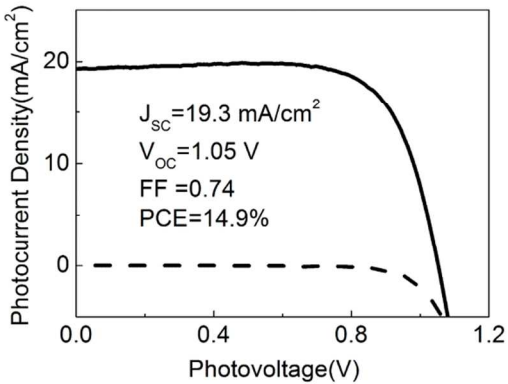


Figure S4. The photocurrent density-photovoltage characteristic of the best-performing planar junction device.

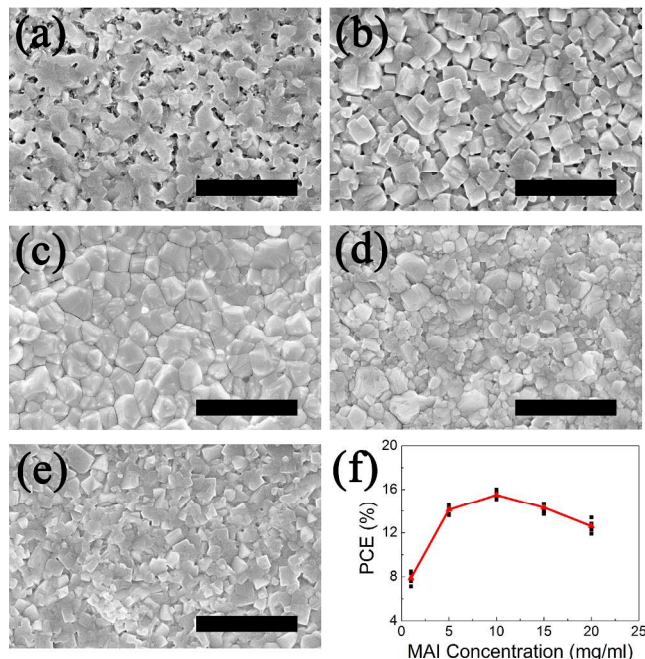


Figure S5. Top-view SEM images (a-e) and device efficiency (PCE) (f) of the MAPbI₃ films prepared with various concentrations of MAI solution. For SEM images, MAI solution concentrations are 1 mg/ml (a), 5 mg/ml (b), 10 mg/ml (c), 15 mg/ml (d) and 20 mg/ml (e), and the scale bar is 1 μ m.

The SEM images of the MAPbI₃ films prepared by different concentrations of MAI solution are shown in Figure S5, while the volume of MAI solution is 400 μ l and the reaction temperature is 80 °C. As shown in Figure S5a and b, low concentration MAI solutions (1 mg/ml and 5 mg/ml) cannot produce compact MAPbI₃ films. The MAPbI₃ film prepared by 10 mg/ml MAI solution exhibits compact structure and well crystalized grains (Figure S5c). After further increasing the concentration (15 mg/ml and 20 mg/ml), the prepared films still have compact structure, but the size of the crystal grains is smaller than that prepared by 10 mg/ml MAI solution (Figure S5d and e).

The PCEs of the devices based on the MAPbI₃ films prepared by different concentration

MAI solutions are summarized in Figure S5f. For 1 mg/ml MAI solution, low average efficiency of 7.9% is obtained. After increasing the concentration to 5 mg/ml, the devices achieve an average efficiency of 14.1%. The devices prepared by 10 mg/ml MAI solution achieve the best average efficiency of 15.5%, which comes from the compact structure and the high crystallization of MAPbI₃ harvester layers. For MAI solutions with high concentration (15 mg/ml and 20 mg/ml), the corresponding devices achieve relatively low average efficiency (14.3% and 12.6%).

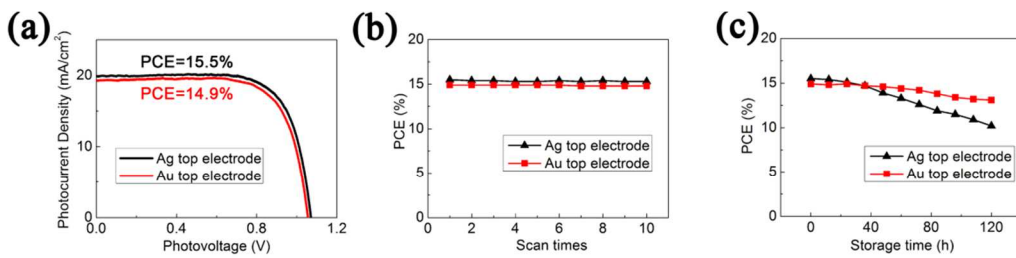


Figure S6. (a) The photocurrent density-photovoltage characteristics of the devices with Ag and Au top electrodes, (b) The relationship between device efficiency (PCE) and scan times, (c) The relationship between device efficiency (PCE) and storage time.

The photocurrent density-photovoltage characteristics of the devices with Ag and Au top electrodes are shown in Figure S6a. The device with Ag electrode exhibits a slightly higher efficiency than the device with Au electrode. It is likely because Ag electrode can reflect light more effectively than Au electrode. The measurement-stability of the devices with Ag and Au top electrodes are shown in Figure S6b. The devices are scanned ten times with 1 min interval. As shown in Figure S6b, the devices show good stability in the repeated measurements. Therefore, the data of devices with Ag top electrodes in our work is credible.

The long term stability of the devices with Ag and Au top electrodes are shown in Figure S6c. The devices are stored in a brown desiccator with silica-gel desiccant. As shown in Figure S6c, the device based on Au electrode shows better stability than that based on Ag electrode during the long term stability test. Therefore, Au top electrode is necessary for the measurement with long period.

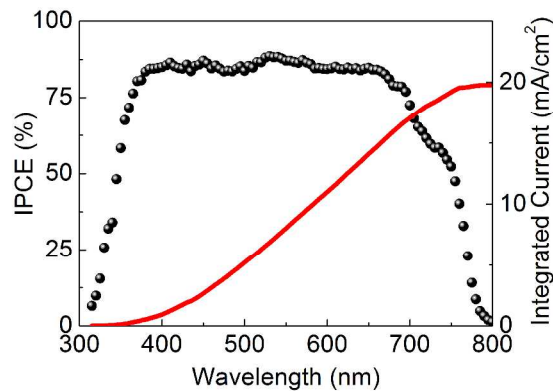


Figure S7. IPCE spectrum (black solid circle) and integrated photocurrent (red line) of the best-performing device.

The photocurrent density from I-V measurement under solar simulator is 20.7 mA/cm^2 , and the photocurrent density from integrating IPCE spectrum is 19.8 mA/cm^2 . The mismatch between these two measurements is less than 5%.

References

- (1) Burschka, J.; Pellet, N.; Moon, S.; Humphry-Baker, R.; Gao, P.; Nazeeruddin, M.; Grätzel, M. Sequential Deposition as a Route to High-Performance Perovskite-Sensitized Solar Cells. *Nature* **2013**, *499*, 316–319.